Block Triangulation using Three-line Images

TIMM OHLHOF, München

ABSTRACT

The most advanced camera concept makes use of 3 linear CCD arrays. Stereo images are acquired quasi simultaneously while the camera platform is moving. The mathematical model of photogrammetric point determination is based on a polynomial approach in case of airborne imagery, whereas orbital constraints should be utilized in case of spaceborne imagery. Computer simulations on point determination have turned out that the most accurate results can be obtained by simultaneous block adjustment of multiple overlapping and additional crossing strips. The usefulness of the 3-line camera concept and the applicability of the proposed mathematical models of point determination have been proven with practical airborne MEOSS and spaceborne MOMS-02 imagery. For both MEOSS and MOMS-02 imagery, empirical accuracies in object space of 1 pixel or better in planimetry and height were obtained as verified by independent check points.

1. THREE-LINE CAMERAS

With the introduction of digital image processing techniques in the last decades revolutionary changes have occurred in photogrammetry. Primary data acquisition, however, largely relies on film based frame cameras, since 2-D CCD arrays with a comparable size and resolution are presently not available, and are not likely to be available in the near future.

High resolution linear CCD sensors are an interesting alternative for aerial and even more so for space photogrammetry. They offer the advantage of direct digital image acquisition, but require more sophisticated processing techniques, because the imagery is taken while the sensor platform is moving. The most advanced camera concept makes use of 3 linear CCD sensor arrays. In this case stereo images are acquired quasi simultaneously. It should be noted that the 3 CCD-lines are imaging different terrain at the same time, whereas the 3 lines image the same terrain at different times, as the sensor platform moves.

In the last few years the 3-line camera concept has been realized for experimental airborne as well as spaceborne projects and is now getting into a pre-operational stage. The main important camera systems based on the 3-line camera concept are:

- Monocular Electro-Optical Stereo Scanner (MEOSS)(Lanzl 1986),
- Modular Optoelectronic Multispectral Scanner (MOMS-02)(Seige, Meissner 1993),
- Digital Photogrammetric Assembly (DPA)(Müller et al. 1994),
- High Resolution Stereo Camera (HRSC)(Neukum, Tarnopolsky 1990),
- Wide-Angle Optoelectronic Stereo Scanner (WAOSS)(Sandau, Bärwald 1994),
- Wide Angle Airborne Camera (WAAC)(Eckardt 1995),
- Triplet Linear Scanner (TLS)(Murai et al. 1995).

MEOSS, DPA, WAAC and TLS are airborne projects, whereas MOMS-02, HRSC and WAOSS are designed for spaceborne applications. A common major objective of all projects is the realization of and the software development for a completely digital photogrammetric processing chain for 3-line imagery from primary data acquisition to the generation of Digital Terrain Models (DTM) and orthoimage maps.

In the following a brief description of the mathematical model of point determination is given, though it should be noted that different approaches are used for airborne and spaceborne imagery. Computer simulations on point determination using HRSC imagery have been performed to obtain a survey of the attainable accuracy if a block of several overlapping strips is adjusted simultaneously. Furthermore,

results of tests with practical airborne MEOSS and spaceborne MOMS-02 imagery are presented. Finally, conclusions are drawn and requirements on 3-line camera projects are formulated.

2. PHOTOGRAMMETRIC POINT DETERMINATION

In this chapter the mathematical model of point determination is described. In case of airborne imagery a polynomial approach is suggested, whereas a new approach which makes use of orbital constraints is proposed in case of spaceborne imagery.

The photogrammetric point determination is based on the principle of bundle adjustment and comprises the determination of object points and the reconstruction of the exterior orientation of the 3-line images. It represents a central task withì in the photogrammetric processing chain on which all subsequent products are based.

The collinearity equations

$$u = u(x, x^c(t), \theta(t)) \tag{1}$$

formulate the relationship between the observed image coordinates $u = (u_x, u_y)^T$, the unknown object point coordinates $x = (X,Y,Z)^T$ of a point P and the unknown parameters of exterior orientation $x^c = (X^c,Y^c,Z^c)^T$ and $\theta = (\zeta,\eta,\theta)^T$, respectively, of the image I_j. The orientation angles ζ, η and θ have to be chosen in such a way that singularities are avoided. In aerial photogrammetry, the roll, pitch and yaw angles are usually used in connection with a topocentric object coordinate system. In space photogrammetry the three Euler angles, which are related to the spacecraft motion along the trajectory, are well suited in conjunction with a geocentric object coordinate system.

2.1 Airborne model

In general, the mathematical model for the reconstruction of the exterior orientation should use 6 unknown parameters for each 3-line image I_j. In practice, however, there is not enough information to determine such a large number of unknowns. The exterior orientation parameters are estimated only for so-called orientation points I_k, which are introduced at certain time intervals, e.g. every 100th readout cycle. In between, the parameters of each 3-line image I_j are expressed as polynomial functions (e.g. Lagrange polynomials) of the parameters at the neighbouring orientation points (Ebner et al. 1994a). This model reduces the number of unknown exterior orientation parameters to a reasonable amount and describes the position and attitude behaviour of the airborne camera platform quite well. For preprocessed position and attitude data, e.g. aquired by differential GPS and INS, observation equations are formulated. Systematic errors of the position and attitute observations are modeled through additional strip- or block-invariant parameters. By limitation to constant and time-dependent linear terms which describe the main effects, 12 additional parameters, namely a bias and a drift parameter for each exterior orientation parameter, are introduced. The position

$$x^c(t) = x^c(t,X^c,b) \tag{2}$$

and attitude

$$\theta(t) = \theta(t,\Theta,\beta) \tag{3}$$

of the camera at selected orientation points including the bias and drift parameters b and β, respectively, yield the modified collinearity equations
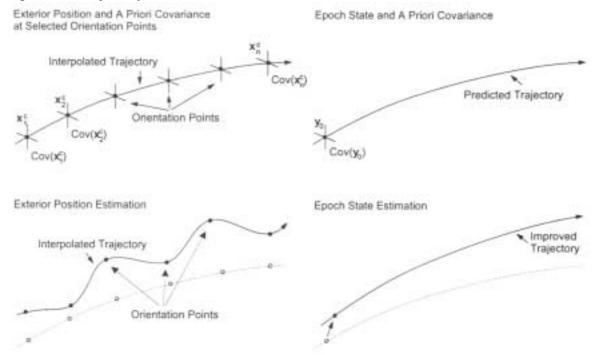
$$\boldsymbol{u} = \boldsymbol{u}\,(x, x^c(t), \boldsymbol{\theta}\,(t)) = \boldsymbol{u}\,(t, x, X^c, \boldsymbol{b}, \boldsymbol{\Theta}, \boldsymbol{\beta}), \tag{4}$$

where x^c and $\boldsymbol{\theta}$ denote the position and attitude vectors at the CCD readout times t, whereas X^c and $\boldsymbol{\Theta}$ comprise position and attitude at the orientation points I_k.

2.2 Spaceborne model

2.2.1 Orbital constraints

The airborne model described above is not recommended for spaceborne applications because the estimated position parameters at subsequent orientation points are not associated with a physical model of the spacecraft trajectory.

To overcome this drawback, the bundle adjustment algorithm is supplemented by a rigorous dynamical modeling of the spacecraft motion to take orbital constraints into account. The camera position parameters x^c, which have been estimated so far at certain time intervals, are now replaced by the 6 parameters of the epoch state vector y_0 and additional force model parameters $\boldsymbol{p}$. The force model parameters $\boldsymbol{p}$ may comprise the drag coefficient C_D and the solar radiation pressure coefficient C_R. Figure 1 demonstrates the fundamental difference between the airborne and the spaceborne model. In the airborne model (left), the position parameters are assumed as independent of the flight behaviour of the spacecraft, which may result in an unrealistic trajectory. However, the spaceborne model (right) exploits the fact that the spacecraft proceeds along an orbit trajectory and all scanner positions lie on this trajectory, when estimating the spacecraft's epoch state vector.

In order to properly utilize the full information contained in the tracking or GPS measurements and in the 3-line imagery, both data types have to be evaluated in a combined adjustment procedure. Due to the complexity of both the orbit determination process and the photogrammetric bundle adjustment a direct combination of the corresponding software packages does not appear to be feasible or adequate. Instead, an approach is presented, which is statistically equivalent to a direct combination of tracking/GPS measurements and image coordinates.

The following information is incorporated into the bundle adjustment as the result of the previous orbit determination process:

- A priori values and covariance matrices of y_0 and p
- Trajectory data x^c, covering the entire imaging session
- Partial derivatives of x^c with respect to y_0 and p

The trajectory data and partial derivatives may be compressed using Chebyshev polynomial approximation.

The spaceborne model has essential advantages for the photogrammetric point determination task, which can be summarized as follows:

- Full utilization of the information contents of the tracking/GPS data in a statistically consistent way.
- A reduced number of unknown exterior orientation parameters, which stabilizes the solution of the reduced normal equations.
- The results of the combined bundle adjustment allow a scientific interpretation of the camera position, as they satisfy the physical laws of motion on a satellite trajectory.

Due to the lack of a dynamical model describing the camera's attitude behaviour during an imaging sequence, it is not possible to introduce attitude constraints into the bundle adjustment in a similar way as the orbital constraints. To this end, the concept of orientation points is maintained for the spacecraft's attitude.

2.2.2 Mathematical model

To include orbital constraints, the camera position and hence the image coordinates have to be expressed as a function of the satellite's epoch state vector y_0 and the force model parameters p :

$$x^c\,(t) = x^c\,(t,y_0,p) \tag{5}$$

Based on this representation, the image coordinates may be written as

$$
\begin{aligned}
u \;&=\; u\,(x,x^c(t),\theta(t)) \\
&=\; u(t,\mathbf{x},y_0,p,\Theta,\beta)\,,
\end{aligned} \tag{6}
$$

while the partial derivatives required in the adjustment are given by

$$\frac{\partial u}{\partial y_0}\,,\quad \frac{\partial u}{\partial x^c}\,\frac{\partial x^c}{\partial y_0} \tag{7}$$

$$\frac{\partial u}{\partial p}\,,\quad \frac{\partial u}{\partial x^c}\,\frac{\partial x^c}{\partial p} \quad\text{and} \tag{8}$$

$$\frac{\partial u}{\partial \Theta}\,,\quad \frac{\partial u}{\partial \Theta}\,\frac{\partial \Theta}{\partial \Theta} \tag{9}$$

Here the partials of x^c with respect to y_0 and p are obtained from the variational equations which are solved simultaneously with the equation of motion. The required partial derivatives (9) are achieved by differentiation of the collinearity equations and the polynomial interpolation formula.

3. COMPUTER SIMULATIONS ON BLOCK TRIANGULATION

3.1 Mars96 mission and the HRSC experiment

In this chapter computer simulations on block triangulation of spaceborne HRSC imagery are presented. The HRSC camera was designed to be flown towards planet Mars on board a Russian spacecraft in 1996. The orbit of the Mars96 spacecraft will be elliptic with a periapsis height of 300 km and an apoapsis height of 22 000 km.

HRSC is a one-lens camera and contains three identical sensor plates in the focal plane which can be called according to the geometric arrangement the forward, the nadir and the backward (looking) plate, respectively. Each plate consists again of 3 CCD sensor arrays (Thompson THX 7808) and each array of 5184 active elements. In the nadir plate the middle (nadir looking) CCD array is a panchromatic channel, the other 2 arrays are green and blue channels. In the forward plate the outermost CCD array represents a panchromatic stereo channel, the innermost array another panchromatic channel for photometric purposes and the middle array an infrared channel. The same is in the backward plate except that the infrared channel is replaced by a purple one. The ground pixel size at periapsis is 12 m for all channels if no formation of macropixels takes place. The photogrammetric processing is mainly based on imagery of the nadir and the two stereo channels. The most important camera parameters of HRSC, MEOSS and MOMS-02 are listed in Table 1. A detailed description of the two stereo camera experiments HRSC and WAOSS and the photogrammetric processing chain is given by Albertz et al. (1993) and Ebner et al. (1994b).

HRSC will operate in the near periapsis region, so that about 10-20 % of the Martian surface can be imaged by HRSC with a ground pixel size of 12-20 m. The block triangulation based on HRSC images therefore implies the simultaneous adjustment of several overlapping strips, which will be aquired around the periapsis with a nearly constant ground pixel size.

Computer simulations on block triangulation have been performed to obtain a survey of the attainable accuracy and to give recommendations in the planning phase of the Mars96 mission. Comprehensive simulations on local, regional and global point determination based on HRSC and WAOSS imagery have been conducted by Ohlhof (1995).

	HRSC	MEOSS	MOMS-02
Sensor parameters			
- Manufacturer	DASA	DLR	DASA
- Number of linear CCD arrays	9	3	7 (8)
- Nominal focal length nadir/stereo [mm]	175.0	61.6	660.0 / 237.2
- CCD element size [μm]	7.0	10.7	10.0
- Number of active pixels per array nadir/stereo	5184	3236	8304 / 5800
- Stereo angle [°]	19.0	23.5	21.4
Flight and image parameters			
- Camera carrier	Spacecraft	Aircraft	Space shuttle
- Flying height [km]	300[b]	11.3[a]	296
- Ground resolution nadir/stereo [m/pixel]	12.0[b c]	2.0[a]	4.5 / 13.5
- Swath width nadir/stereo [km]	62[b]	6.4[a]	37 / 78

Table 1: Technical parameters of the stereo scanners HRSC, MEOSS and MOMS-02 ([a] during the testflights in 1989, [b] at periapsis, [c] without macropixel formation).

3.2 Input parameters

The computer simulations were performed for 5 different block configurations:

- Single strip (for reasons of comparison)
- Block of 2 strips with $q = 40$ % side overlap
- Block of 3 strips with $q = 60$ %
- Block of 10 strips with $q = 60$ %
- Block of 10 strips with $q = 60$ % and 4 additional crossing strips (Figure 2)
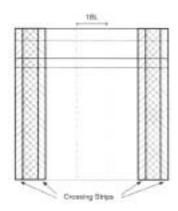

Figure 2: Block consisting of 10 strips with 5 baselenghts each and 60 % side overlap as well as 4 additional crossing strips at the border of the block.

The strip length was chosen to 5 baselengths (510 km). This results in the fact that points at the beginning and the end of the single strip are projected into 2 images only, whereas every point in the central part of the strip is projected into 3 images. The object coordinate system is defined as topocentric Cartesian system XYZ with the positive direction of the X-axis parallel to the direction of flight.

The object points are arranged in a grid with $\Delta X = 0.8$ km, $\Delta Y = 15.5$ km and $Z = 0$ km. For each block configuration, the image coordinates of the object points were computed assuming a straight forward flight path with a constant altitude of 300 km. All image coordinates were treated as being uncorrelated with equal standard deviations of 2 μm (0.28 pixel size).

For each orientation point attitude observations were introduced with a relative accuracy of 4", assuming gyro readings during the HRSC imaging sequence. The distance between the orientation points was chosen to 800 rows (ca. 10 km). All positions were constrained to lie on the orbit trajectory. No ground control information was used. The datum was defined using the method of free adjustment, being characterized by a minimization of the trace of the covariance matrix of the adjusted object point coordinates.
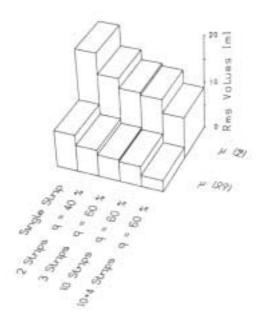
3.3 Results

Figure 3: Rms values $\mu_{\hat{X}\hat{Y}}$ and $\mu_{\hat{Z}}$ for 5 different block configurations (HRSC).

For analysis, the rms values $\mu_{\hat{X}\hat{Y}}$ (planimetry) and $\mu_{\hat{Z}}$ (height) of the theoretical standard deviations $\sigma_{\hat{X}}$, $\sigma_{\hat{Y}}$ and $\sigma_{\hat{Z}}$ of all adjusted object point coordinates were calculated. The rms values represent the local or interior accuracy of point determination. In Figure 3 these rms values are shown graphically for the 5 block configurations.

It can be seen from Figure 3 that the planimetric and height accuracies improve if more than one strip is adjusted simultaneously. What is more, the accuracies improve with increasing side overlap. For $q = 40$ % each object point is projected into 3.2 image strips on average and for $q = 60$ % into 4.3 image strips. If a block of 10 overlapping strips is adjusted, accuracies of 4.3 m and 11.8 m can be achieved in planimetry and height respectively. The geometric strength of the block and hence the accuracy of point determination can be improved considerably, if 4 crossing

strips are added at the borders of the block (Figure 4). Each object point is projected into at least 3 image strips and the rms values amount to 2.4 m (0.2 pixel) in planimetry and 8.9 m (0.7 pixel) in height.
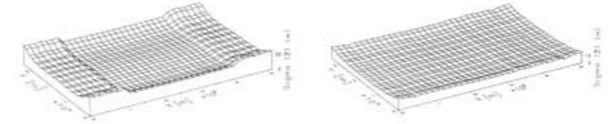

Figure 4: Standard deviations of the adjusted $\hat{Z}$-coordinates of the object points for the 10 strip-block without (left) and with (right) 4 additional crossing strips (HRSC).

4. PRACTICAL TESTS USING MEOSS AND MOMS-02 IMAGERY

In this chapter, results obtained by photogrammetric processing of practical airborne and spaceborne 3-line imagery are presented. The airborne imagery was acquired by the MEOSS camera and the spaceborne imagery by the MOMS-02 camera.

For both projects the available ground points were divided into two groups in order to compute the empirical accuracy of point determination for quality control. The first group consists of 12 control points, where 3 points each are located in the corners of the threefold (MOMS-02) and sixfold (MEOSS) overlapping area, respectively, to ensure a precise definition of the global datum for the following quality control. The second group comprises 45 (MEOSS) and 42 (MOMS-02) geometrically well distributed points, respectively, which were used as check points.

For all check points the rms values of the theoretical and empirical accuracies were computed. The theoretical values were calculated from the inverted normal equations and the a posteriori $\hat{\sigma}_0$ value of the bundle adjustment. The empirical values were derived by comparing the estimated object coordinates of the check points and the known values.

4.1 Evaluation of airborne MEOSS imagery

It was the year 1981 when the German Aerospace Research Establishment (DLR) proposed to participate in an Indian satellite mission with MEOSS. Unfortunately, the MEOSS experiment was not successful due to launcher failures in 1988 and 1993. Since 1986, however, some successful airborne test flights took place using an engineering model (1986) and the 2nd flight model (1989).

MEOSS has a single lens with a focal length of 61.6 mm and 3 CCD sensor arrays. Each CCD array comprises 3236 sensor elements with 10.7 μm size (Table 1). The imagery of the last airborne test flight was taken in June 1989 and depicts a rural area near Dorfen about 40 km to the east of Munich. Six image strips, three from the North-South (NS) flight path, and three from the West/East (WE) flight path respectively, with a five- and sixfold overlapping area were acquired and processed.

The bundle block adjustment was performed in a topocentric coordinate system with X and Y as planimetric coordinates and Z as height coordinate. The image coordinates of the conjugate points were automatically derived from digital image matching, whereas the image coordinates of the ground control points (GCP) and check points were measured interactively (Heipke et al. 1994). The ground coordinates of the GCP and check points were obtained by conventional aerotriangulation using two analog frame images of scale 1:15 000. Position data were recorded by the aircraft navigation system and an Inertial Navigation System (INS) provided attitude information. The distance between the orientation points was derived by analyzing the given INS data. Based on this analysis an optimum distance of 40 rows was chosen, corresponding to a flight distance of 80 m and a flight time of 0.42 s.

The following data were incorporated as observations in the bundle block adjustment:

- Image coordinates of 15 799 conjugate points ($\sigma = 0.25$ pixel),
- Image coordinates of 12 GCP ($\sigma = 0.4$ pixel),
- Image coordinates of 45 check points ($\sigma = 0.4$ pixel),
- Object coordinates of 12 GCP ($\sigma_X = \sigma_Y = 0.33$ m, $\sigma_Z = 0.48$ m),
- Position parameters at 423 orientation points ($\sigma_X^c = \sigma_Y^c = \sigma_Z^c = 20$ m),
- Attitude parameters (ζ, η, θ) at 423 orientation points ($\sigma_\zeta = \sigma_\eta = 162''$).

MEOSS		theor.	empir.
$\mu_{\hat{X}}$	[m]	1.0	1.1
$\mu_{\hat{Y}}$	[m]	1.0	0.9
$\mu_{\hat{Z}}$	[m]	3.1	2.0

Table 2: Rms values $\mu_{\hat{X}}, \mu_{\hat{Y}}, \mu_{\hat{Z}}$ of the theoretical and empirical accuracies derived from 45 check points.

Table 2 contains the rms values of the theoretical and empirical accuracies for all 45 check points. The empirical standard deviations show that accuracies of 1 m (0.5 pixel) in planimetry and 2 m (1 pixel) in height were achieved. The good correspondence between the theoretical and the empirical values proves the correctness of the stochastic and the functional model. A further analysis of the results is given by Heipke et al. (1994).

4.2 Evaluation of spaceborne MOMS-02 imagery

The MOMS-02 camera was launched on April 26, 1993 as part of the 2nd German Spacelab mission D2. The optical system of MOMS-02 consists of a stereo module and a multispectral module. The 3 lenses of the stereo module with 1 CCD sensor array (Fairchild 191) each provide threefold along track stereo scanning with different ground resolutions. The nadir looking CCD array (4.5 m ground pixel size) comprises 2 arrays with 6000 sensor elements each, which are optically combined to 1 array with 8304 active sensor elements. The other CCD arrays of the stereo module consist of 5800 active sensor elements (13.5 m ground pixel size) (Table 1).
To verify the concept of orbital constraints in the bundle adjustment, one imaging sequence with three image strips and 32120 rows each covering 430×78 km^2 West Australia (orbit #75B, mode 1) has been selected.
The bundle adjustment was performed in the geocentric coordinate system WGS84. About 14 000 conjugate points were found automatically using nearly the same image matching procedure as applied to the MEOSS imagery. In the area covered by the three image strips 79 DGPS-derived ground points were available with a standard deviation of 0.1 m. 69 points including 12 GCP and 42 check points were identified in the images and measured stereoscopically using a softcopy photogrammetric workstation.
During the D2 mission tracking was routinely performed using the Tracking and Data Relay Satellite System (TDRSS). The orbit determination for orbit #75B was based on 900 S-Band Doppler measurements with a sampling rate of 10s covering about 180 minutes. The pure statistical standard deviations of the epoch state vector components were 30 m, whereas unmodeled accelerations of the attitude thruster system add an error of up to 50 m (Braun, Reigber 1994).
A major problem arose from the fact that the image recording times could in general not be related better than 0.5 s to the time scale UTC. A time offset of 0.5 s corresponds to an along-track position offset of the space shuttle of 0.5 s $\cdot$ 7 km/s = 3.5 km (!). Since no parameter for the time offset exists in

the bundle adjustment algorithm, a realistic weighting matrix for the epoch state vector components has been derived to relax the orbital constraints in the along-track direction (Gill et al. 1995). The force model parameters p were treated as constants due to the short time span (1 min) of image acquisition. Attitude information was derived from gyro recordings of the Inertial Measurement Units (IMU) of the shuttle Guidance Navigation and Control System. Based on approximation tests the optimum distance between two orientation points was found to be 4615 rows, corresponding to a flight distance of 62.3 km and a flight time of 9.1 s.

The following data were introduced as observations:

- Image coordinates of 13 959 conjugate points (σ = 0.3 pixel),
- Image coordinates of 12 GCP (σ = 0.5 pixel),
- Image coordinates of 42 check points (σ = 0.5 pixel),
- Object coordinates of 12 GCP (σ_X, σ_Y, σ_Z = 0.1 m),
- Epoch state vector components with associated 6×6 weighting matrix,
- Attitude parameters (ζ, η, θ) at 8 orientation points (σ_ζ, σ_η, σ_θ = 50 ″).

MOMS-02		theor.	empir.
$\mu_{\hat{X}}$	[m]	14.9	12.4
$\mu_{\hat{Y}}$	[m]	15.1	12.2
$\mu_{\hat{Z}}$	[m]	10.4	13.0

Table 3: Rms values $\mu_{\hat{X}}$, $\mu_{\hat{Y}}$, $\mu_{\hat{Z}}$ of the theoretical and empirical accuracies derived from 42 check points.

In Table 3 the rms values of the theoretical and empirical accuracies of the check point coordinates $\hat{X}$, $\hat{Y}$ and $\hat{Z}$ are presented. The empirical values show that accuracies of about 12 m (0.9 pixel) in X, Y and Z were obtained. What is more, a graphical analysis of the residuals in the check points showed that the results are not affected by systematic errors.

Due to the improper time synchronization between image and orbit data, large corrections to the a priori state vector components occured, that contribute mainly to along-track position errors. The orbit accuracy from the pure TDRSS solution (50-70 m) could therefore not be improved. A high accuracy orbit determination from a combined evaluation of image and tracking data requires a time synchronization of 0.1 ms or better. The results are discussed in more detail in Gill et al. (1995) and Ohlhof (1995).

5. CONCLUSIONS

Three-line cameras provide full stereo capability. Full 3D information of the terrain surface can be derived from this kind of imagery. Investigations on point determination using simulated and practical imagery prove the usefulness of the 3-line camera concept for airborne as well as spaceborne applications. The mathematical model of bundle adjustment is based on a polynomial approach in case of airborne imagery, whereas orbital constraints should be utilized in case of spaceborne imagery.

The evaluation of practical MEOSS and MOMS-02 imagery shows that empirical accuracies in object space of at least 1 pixel in planimetry and height can be achieved with a few GCP. In order to obtain subpixel accuracies with a limited number of or even without GCP,

- a large number of conjugate points derived from image matching,
- highly accurate observations for position/orbit and attitude (GPS, tracking data, INS),

- a high precision time synchronization between the recorded imagery and the position/orbit and attitude observations, and
- a block configuration with many overlapping ($q \ni 60\ \%$) and possibly additional crossing stripsare required.

6. ACKNOWLEDGEMENTS

7. REFERENCES

Albertz J., F. Scholten, H. Ebner, C. Heipke and G. Neukum (1993): Two Camera Experiments on the Mars94/96 Missions. GIS, Vol. 6, No. 4, pp. 11-16.

Braun C.v. and C. Reigber C. (1994): Space shuttle orbit determination using empirical force modelling of attitude maneuvers for the German MOMS-02/D2 mission. Flight Mechanics and Estimation Theory Symposium, Goddard Space Flight Center, May 17-19, Greenbelt.

Ebner H., W. Kornus and T. Ohlhof (1994a): A simulation study on point determination for the MOMS-02/D2 Space Project using an extended functional model. GIS, Vol. 7, No. 1, pp. 11-16.

Ebner H., T. Ohlhof and L. Tang (1994b): Eine Studie zur Bildzuordnung und Punktbestimmung im Rahmen der Mars94-Mission. ZPF, Vol. 62, No. 2, pp. 57-71.

Eckardt A. (1995): The performance of the new Wide Angle Airborne Camera (WAAC). Int. Arch. of Photogrammetry and Remote Sensing, Vol. 30, Part 5W1, pp. 26-29.

Gill E., O. Montenbruck, T. Ohlhof and M. Schmidhuber (1995): First results on shuttle orbit adjustment using MOMS-02 imagery. Proceedings of the International Space Dynamics Symposium, June 19-23, Toulouse.

Heipke C., W. Kornus and A. Pfannenstein (1994): The evaluation of MEOSS airborne 3-line scanner imagery - processing chain and results. Int. Arch. of Photogrammetry and Remote Sensing, Vol. 30, Part 4, pp. 239-250.

Lanzl F. (1986): The Monocular Electro-Optical Stereo Scanner (MEOSS) satellite experiment. Int. Archieves of Photogrammetry and Remote Sensing, Vol. 26, Part 1, pp. 617-620.

Montenbruck O., E. Gill and T. Ohlhof (1994): A Combined Approach for Mars-94 Orbit Determination and Photogrammetric Bundle Adjustment. DLR-Forschungsbericht 94-13, 95 p.

Müller F., O. Hofmann and A. Kaltenecker (1994): Digital Photogrammetric Assembly (DPS) point determination using airborne three-line camera imagery: practical results. Int. Arch. of Photogrammetry and Remote Sensing, Vol. 30, Part 3/2, pp. 592-598.

Murai S., Y. Matsumoto and X. Li (1995): Stereoscopic imagery with an airborne 3-line scanner (TLS). Int. Arch. of Photogrammetry and Remote Sensing, Vol. 30, Part 5W1, pp. 20-25.

Neukum, G. and V. Tarnopolsky (1990): Planetary Mapping - The Mars Cartographic Data Base and a cooperative Camera Project for 1994. GIS, Vol. 3, No. 2, pp. 20-29.

Ohlhof T. (1995): Lokale, regionale und globale Punktbestimmung mit Bild- und Bahninformation der Mars96-Mission. PhD thesis, Technical University Munich (in print).

Sandau R. and W. Bärwald (1994): A three-line wide-angle CCD stereo camera for Mars-94 mission. Int. Arch. of Photogrammetry and Remote Sensing, Vol. 30, Part 1, pp. 82-86.

Seige P. and D. Meissner D. (1993): MOMS-02: An advanced high resolution multispectral stereo scanner for Earth observation. GIS, Vol. 6, No. 1, pp. 4-11.